JOURNAL OF APPLIED ELECTROCHEMISTY 6 (1976) 107–118

Cyclic charge-discharge behaviour of sintered plate and planar cadmium electrodes

R. BARNARD, K. EDMONDSON, J. A. LEE, F. L. TYE

Ever Ready Co. (Holdings) Ltd., *Central Laboratories., St. Ann's Road, London N15 3TJ*

Received 18 January 1975

The cyclic charge-discharge behaviour of sintered plate and planar cadmium electrodes has been studied using galvanostatic and potentiostatic sweep techniques. The cycling inefficiency of sintered electrodes reflected more the discharge process as shown by analytical monitoring of cadmium levels before and after charge. The effect of discharge rate on cycling efficiency was also investigated. Open-circuit recovery experiments indicated that a critical potential was reached at which passivation occurs subsequent to which a plateau region was observed for sintered electrodes. Potentiostatic sweeps on partially discharged electrodes and X-ray diffraction suggested the formation of a nickel-cadmium alloy during charge.

Comparison of cyclic sweeps on sintered and planar electrodes showed the distribution effects of active material through the sinter and also the improved charge acceptance of sintered electrodes. Cyclic sweeps on planar electrodes indicated the involvement of forms of cadmium of different activity, whilst cathodic sweeps after prolonged retention at potentials anodic to passivation indicated a more complex reduction route.

1. Introduction

Recently the charge and discharge behaviour of sintered cadmium electrodes has been restudied [1]. The conclusions drawn were that in early cycle life the cadmium crystallites increase in size concurrent with a redistribution of material within the sinter matrix. The monitoring of residual cadmium levels after discharge and corresponding cadmium hydroxide contents after charge indicated that the early drastic loss in available capacity although interrelated to both charge and discharge processes reflected more the inefficiencies of discharge. This is contrary to the findings of Will and Hess [2]. In early cycles they detected large (1–2 μm) $Cd(OH)_2$ crystals many of which were observed not to reduce easily on charge. Will and Hess's single pore simulation of a battery plate conformed essentially to a planar electrode, and it will be established in this communication that the relative charge acceptance by such electrodes is substantially less than by porous electrodes. Several workers [1, 3, 4] have observed that under regimes of high charge rate by which charging inefficiencies are minimized the delivered capacities appear to be independent of rates of discharge. This implies that discharge failure mechanisms involving restricted diffusion pathways such as pore and pore mouth blockage invoked by Casey and Vergette [5] and Pryzbyla Ramsey and O'Nan [6] may not be valid. Dunning, Bennion and Newman [7] and Bro and Kang [8] concede that their solution diffusion and sinter choking models respectively fail to describe the discharge behaviour. It is recognized, however, that at very high rates of discharge as discussed by Selanger [9] diffusion limitations are manifest.

The formation of a passivating film on oxidation of a planar cadmium electrode has been demonstrated [10]. The composition and mode of formation of the film is not yet resolved. Okinaka [11] prefers a dissolution precipitation process, whereas Armstrong and West [10] argue in favour of a solid state growth process. Both sets of workers consider the film to be β-$Cd(OH)_2$ whereas Brieter and Weinniger [12] and Devanathan and Lakshmanan [13] suggested a CdO layer.

In view of the controversy still surrounding the

behaviour of planar cadmium electrodes in potassium hydroxide and the inadequate analysis of the porous cadmium electrodes the investigations described in this communication were undertaken. It involved primarily galvanostatic and potentiodynamic approaches to both types of electrode.

2. Experimental

2.1. *Materials*

The electrodes were made from nickel sinter and impregnated with $Cd(OH)_2$ after the methods of Fleischer [14] and Horn [15]. The test samples were of the dimensions 10 x 10 x 0·65 mm and contained 0·096 ± 0·005 g of $Cd(OH)_2$ (theoretical capacity 36·2 mAh). The electrodes were also found to contain ~1–4% $Ni(OH)_2$ impurity arising from corrosion of the nickel sinter during preparation. In certain experiments electrodes were impregnated with a uniform mixture of $Cd(OH)_2$ and $Ni(OH)_2$ in order to deliberately increase the level of the latter component to 10–11% of the initial active material weight.

The cadmium disc electrode of 99·999% purity (0·28 cm^2) was sheathed in tightly fitting PTFE tube and polished using alumina before use.

The electrolyte (30% w/w KOH) was prepared from L.R.B. Pearce, Technical Grade Flake and singly distilled water.

2.2. *Galvanostatic cycling*

Charge-discharge curves during the early cycles were obtained manually although an electronic cut-off device set at −200 mV was used to prevent over discharge. Charging was stopped once the steady-state hydrogen evolution plateau had been reached. Extended cycling was performed using automatic equipment described previously [1]. The charge and discharge cut-off levels were fixed at −1050 and −200 mV respectively. The electrodes used with this apparatus were subjected to a standard 'formation' treatment of charging at the $C/2$ rate for 16 h prior to cycling. Charge-discharge curves were displayed using a Smiths 'Servoscribe' single channel or a Speedomax 'W' Multipoint recorder. Constant currents were supplied by conventional transistorised devices. The test cells were of the polypropylene type described previously [1] or similar to that used in the voltammetric measurements described below. Potentials throughout are referred to Hg/HgO/30% KOH.

2.3. *Voltammetric measurements*

The double H-shaped glass cell incorporated nickel-grid counter electrodes placed either side of the working electrode. The Hg/HgO reference electrode incorporated the usual Luggin capillary and the cell electrolyte was continuously purged with nitrogen.

Linear and cyclic sweeps were performed using a Chemical Electronics Potentiostat, (TR40/3A) and linear sweep unit, LSU1 in conjunction with an x–t (Servoscribe) or x–y recorder (Bryans 21004).

Because the sintered plate electrode generated high peak currents (~300 mA) it was necessary to correct the voltammograms for the effect of ohmic drop between the working and reference electrodes. The solution resistance determined by impedance and fast pulse techniques was found to be ~0·3 Ω. Currents and potentials were corrected using an extension of the method described by Delahay [16]. If ν is the applied potential sweep rate, and the actual potential-time function experienced by the working electrode can be approximated by two linear portions having slopes ν' and ν'' then the currents along the ascending branches of the curve and at the peak need to be increased by a factor $(\nu/\nu')^{1/2}$ whilst those along the descending branches must be decreased by a factor $(\nu/\nu'')^{1/2}$. The assumption that the peak current varied as a function of the square root of the sweep rate was found to be valid at slow sweep rates.

Although the correction procedure was only very approximate, it gave a more meaningful shape to the voltammograms. No quantitative significance was attached to the absolute magnitude of the corrected currents. In the case of peak currents <100 mA the current correction factors were ignored since they produced only minor changes to the shapes of the voltammograms.

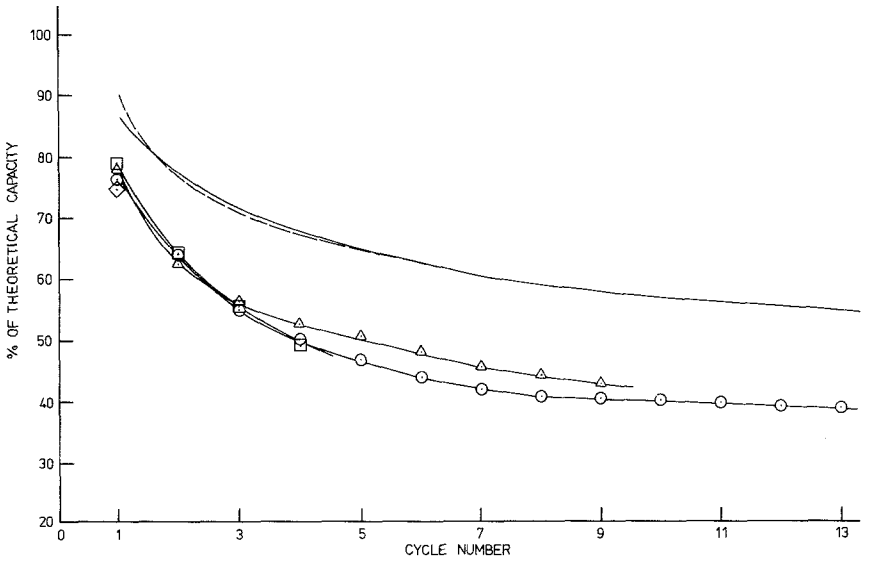

Fig. 1. Delivered discharge capacity versus cycle number. Symbol data, $C/2$ charge (no overcharge formation). ○ $C/1$ discharge rate; △ $C/4$ discharge rate; □ $C/16$ discharge rate; ◇ $C/64$ discharge rate. Continuous line, $C/1$ charge rate, $C/1$ discharge rate after formation at $C/2$ for 16 h; dotted line, $C/1$ charge rate, $C/8$ discharge rate after formation at $C/2$ for 16 h.

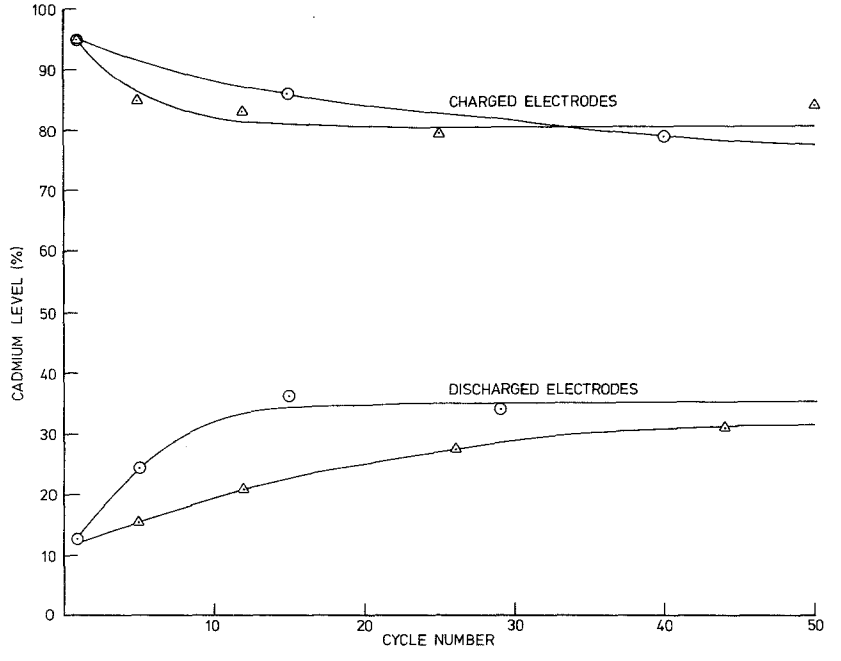

Fig. 2. Levels of cadmium metal determined by chemical analyses of sintered cadmium electrodes. Charge rate $C/1$. ○ $C/1$ discharge rate; △ $C/8$ discharge rate.

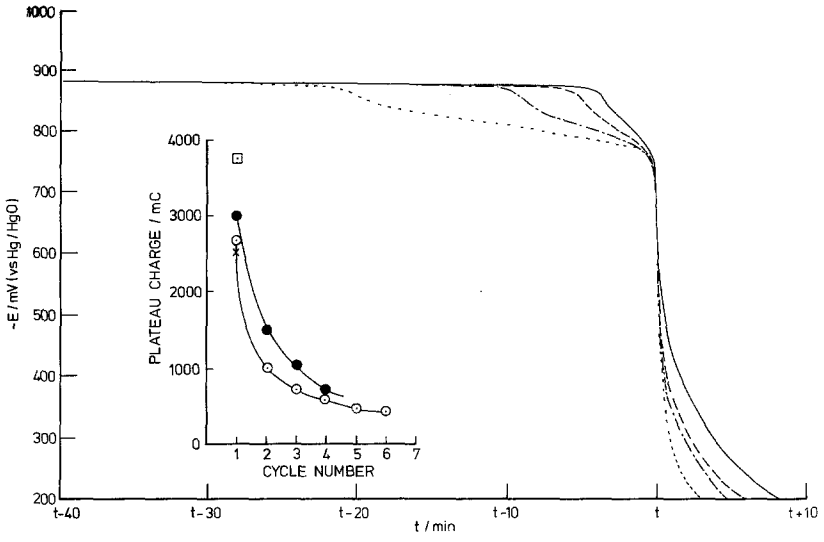

Fig. 3. Galvanostatic discharge profiles ($C/16$ rate) after $C/2$ charge for sintered cadmium electrode. -------- 1st cycle; —·—·— 2nd cycle; — — — — 3rd cycle; ———— 4th cycle. Insert: variation of plateau charge with discharge rate and cycling. $C/2$ charge rate: ○ $C/4$ discharge rate; ● $C/16$ discharge rate; × $C/32$ discharge rate; □ $C/64$ discharge rate.

2.4. *Analytical*

Levels of Cd and $Cd(OH)_2$ in charged and discharged electrodes were determined as described previously [1].

X-ray diffraction patterns were obtained on a Phillips Diffractometer using Ni-filtered, CuK_α radiation (45 kV) under a scan rate of $\frac{1}{2}^\circ$ min^{-1}. Charged or partially charged electrodes were washed with water, IMS and dried under vacuum and coated with polyurethane varnish to prevent aerial oxidation. The test samples were prepared in a glove-box filled with nitrogen. The varnish was found to introduce a broad background hump at low 2θ angles. Patterns were measured by reflecting the incident beam from the surface of the whole electrode.

3. Results and discussion

3.1. *Galvanostatic studies*

Fig. 1 depicts the delivered capacity at different discharge rates as a function of early cycle life at a fixed charge rate of $C/2$. Also included in Fig. 1 are data, previously reported [1], pertaining to a fixed but higher charge rate for electrodes additionally subjected to overcharge during formation ($C/2$ for 16 h). Both sets of data demonstrate the sharp loss in performance in the first few cycles and the apparent insensitivity of the behaviour to the rate of discharge. The difference in the first cycle capacities in the two sets of data reflects the improved charge acceptance of the previous electrodes and is due mainly to the formation overcharge and better distribution of active material.

Monitoring of cadmium metal levels in discharged states for $C/1$ and $C/8$ discharge rates, but under a fixed charge regime, Fig. 2 implies some dependence of discharge performance on discharge rate after, but not for, the first discharge. The impaired charge acceptance of the $C/8$ discharged electrode (upper part of Fig. 2) negates to some extent its improved discharge capacity. The crystallite size of the $Cd(OH)_2$ precipitate and/or its distribution may vary with discharge rate influencing the charge intake. The net affect is to attenuate the influence of discharge rate although it must be stressed that this is not so for the first cycle and negligible after 50 cycles. The discharge process must play a significant role in the poor performance. X-ray diffraction analyses of discharged electrodes after the first and tenth cycles indicated only the hexagonal structure of β-$Cd(OH)_2$. The participation of the secondary sheet structure form of β-$Cd(OH)_2$, claimed by Appelt [17] to be electrochemically inactive, is

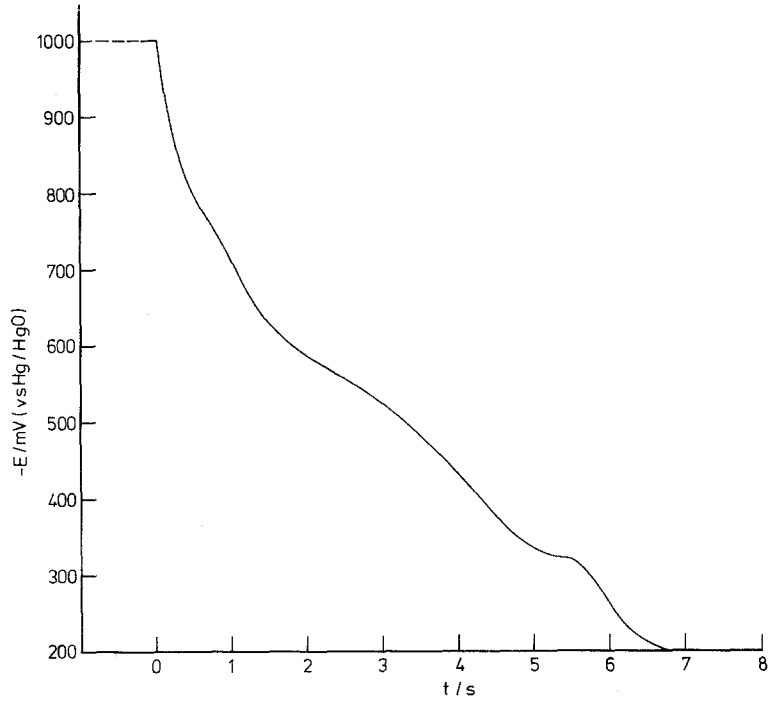

Fig. 4. Galvanostatic discharge curve for unimpregnated nickel sinter electrode at $C/1$ discharge rate after 16 h charge at $C/2$ rate.

not thought to be contributory to the discharge failure mechanism in early cycles as the ratio of the 001/100 intensities indicated its absence. However, after considerable cycling, ~200 cycles, it was detected.

A 100 mV step in the potential profiles appears in the galvanostatic discharge curves from −850 to −750 mV, Fig. 3. The quantity of charge associated with the plateaux is essentially independent of discharge rate (insert, Fig. 3) and it could be conceived as the specific charge required to passivate or block off the remaining active surface. Certainly the plateaux lengths diminish with cycle number consistent with less subsequent cadmium surface to be blocked off. Discharge current interruptions made cathodic to −870 mV followed by an open circuit stand for one hour induced a prolongation of active dissolution for sintered and planar electrodes. It is interpreted, as were earlier potentiostatic [18] and impedance measurements [19], in terms of the diffusion of soluble cadmium species away from the electrode surface delaying the onset of passivation. It is of significance that discharging sintered electrodes to potentials beyond −870 mV followed by the stand on open circuit, however, failed to extend the useful discharge life. This irreversible loss of active material is considered to be due to passivation of the remaining cadmium. The open circuit stand period exerted no influence upon the subsequent plateau region. Pore blockage is therefore an unlikely cause of the plateaux since some dissolution of precipitated $Cd(OH)_2$ is expected on stand under the conditions of excess electrolyte employed in these investigations.

Falk [20] proposed that the end of discharge curve profiles reflected the oxidation of adsorbed hydrogen on the nickel sinter. Samples of unimpregnated nickel sinter were charged at the $C/2$ rate for 16 h and then discharged at the $C/1$ and $C/50$ discharge rates. Fig. 4 shows the discharge curve obtained at the former rate. The sloping region from ~−0·9 V to −0·3 V corresponds with the oxidation of hydrogen [21]. From a knowledge of the nickel sinter area as measured by mercury porosimetry, the charge densities were 360 and 640 $\mu C\,cm^{-2}$, approximately the order expected for monolayer coverage of adsorbed hydrogen. However, the coulombic charge associated with the plateaux was up to two orders of

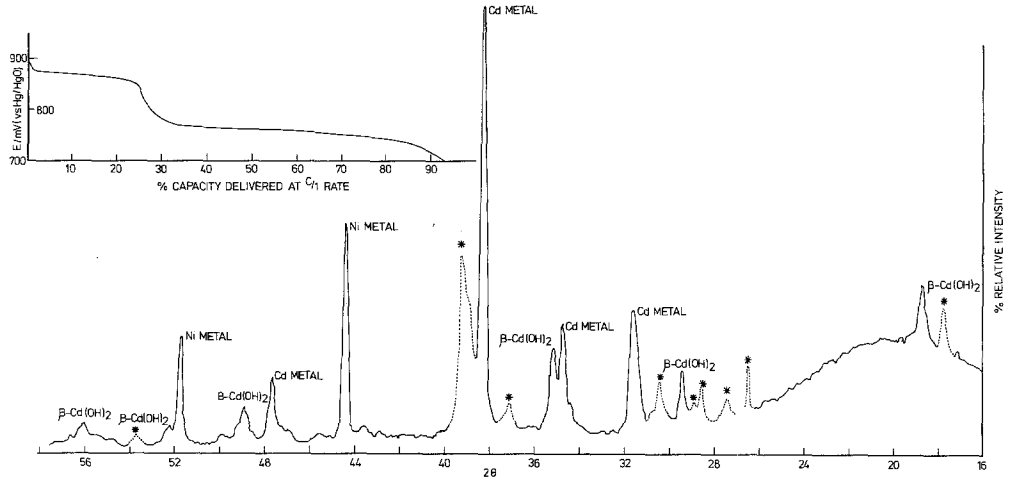

Fig. 5. X-ray diffraction pattern of cadmium sintered electrode after charge for 420 h at $C/1$ rate at 75°C. Insert: stepped galvanostatic discharge profile after charge at $C/1$ rate for 280 h.

magnitude larger thereby eliminating the hydrogen adsorption hypothesis.

Pozin and Terent'ev [22] reported stepped potential-time curves resembling those in Fig. 3 and suggested the discharge of a less active cadmium associated with nickel within the region. They proposed a nickel/cadmium alloy, Ni_5Cd_{21}, without direct confirmation of its presence. Deliberate addition of $Ni(OH)_2$ to the electrode effected a proportional increase in the plateaux lengths and the latter also extended to limiting values on overcharge. These observations are consistent with the formation of an alloy during charge as proposed by Levina and Rozenzweig. [23] .The decrease in plateaux lengths with cycling presumably reflects progressively less reduction of Ni^{2+} on charge. An X-ray diffraction analysis was made on electrodes (containing initially ~10% $Ni(OH)_2$) subjected to extensive overcharge at 75°C, conditions claimed to favour the formation of an alloy, Fig. 5. The pattern indicated the presence not surprisingly of nickel and cadmium metal. Additional lines evident were not characteristic of $Ni(OH)_2$, $CdCO_3$ or K_2CO_3 the most intense being, at a 2θ value of ~39·5° concurrent with an extended stepped discharge profile, insert Fig. 5. Diffraction data have not been published by Pozin and Terent'ev, and the early work by Ekman [24] is considered unreliable. The presence of the γ-brass structure of Ni_5Cd_{21} cannot therefore be confirmed or otherwise as yet. Significantly, thin films of cadmium electrodeposited onto a planar nickel substrate produce a major anodic peak at −750 mV, in line with the lower part of the potential step and the decreased activity of the cadmium [21]. A consideration of the difference in the work functions of nickel and cadmium in the Kolb, Przasnyski and Gerischer [25] model of a metal deposited upon a foreign substrate metal fails to predict a 100 mV depression of potential. This further substantiates alloy formation.

3.2. *Potential sweeps on planar electrodes*

Fig. 6a shows typical first cycle sweep behaviour between −1000 and −750 mV. The single anodic peak at −860 mV relates to the active dissolution of cadmium followed by passivation. Good evidence for the presence of a film at this potential has recently been presented by Armstrong and Edmondson [19] by low frequency impedance measurements. Previous data presented in support of a solid state growth mechanism for the formation of the passivating film [10], namely an apparent independence of the passivation potential on convective conditions, is not conclusive since the rotation measurements should have corresponded with steady state rather than dynamic potential conditions. (Consideration of peak potentials and currents in this work with Armstrong and West's [10] also indicates a labelling error in their Fig. 8). However, measurements at rotation speeds of 2 and 30 Hz in this work

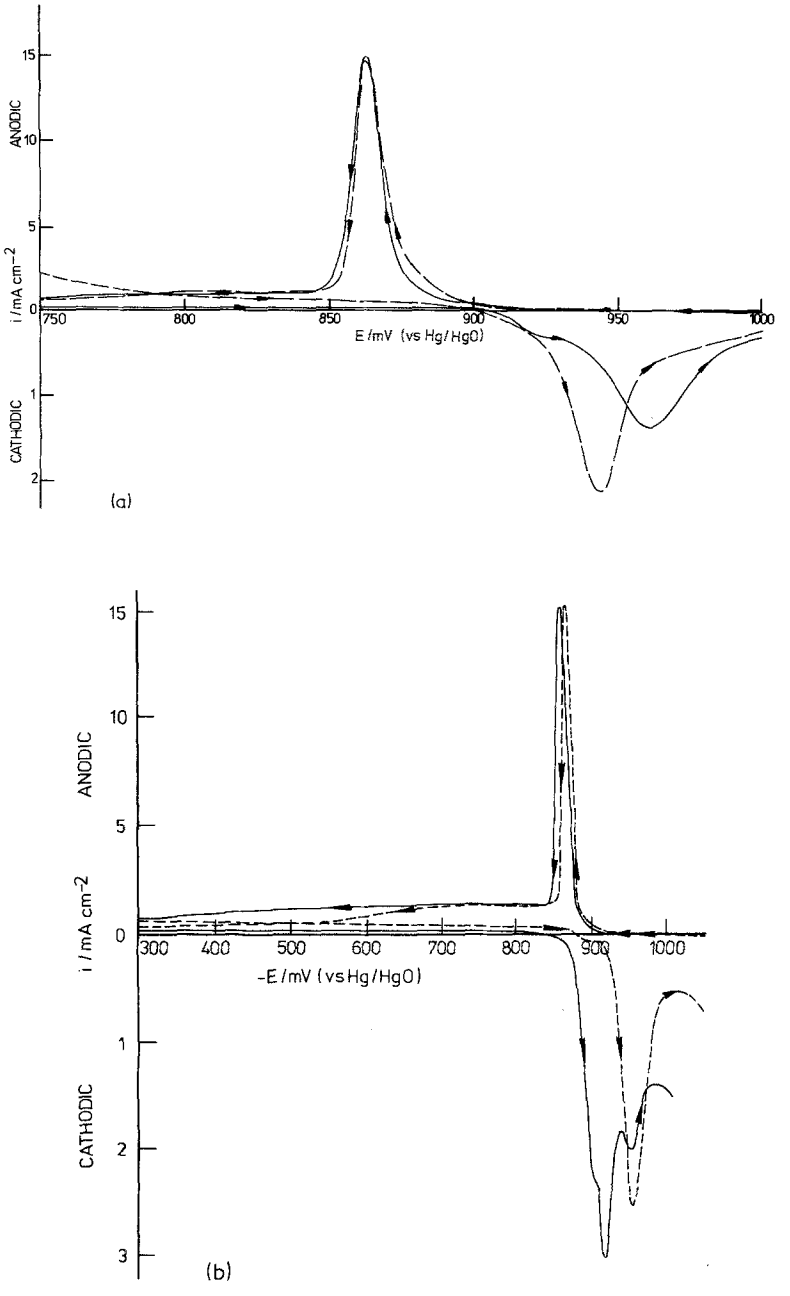

Fig. 6. (a) First cycle potential sweep for planar cadmium electrode; sweep speed 125 mV min^{-1}. – – – – – normal cyclic sweep; ———— electrode held at −750 mV for 1 h before reversal. (b) First cycle potential sweep for planar cadmium electrode; sweep speed 150 mV min^{-1}. – – – – – – normal cyclic sweep; ———— electrode held at −300 mV for 3 h before reversal.

indicate invariance of the steady state peak potential in line with a solid state model of passivation. A distinction between solid state and dissolution-precipitation mechanisms may not be possible, as an extremely fast rate of precipitation might produce the same insensitivity to the change in rotation speeds employed.

The magnitude of the corresponding cathodic peak at −945 mV indicates significant levels of unreduced β-$Cd(OH)_2$ at completion of the sweep.

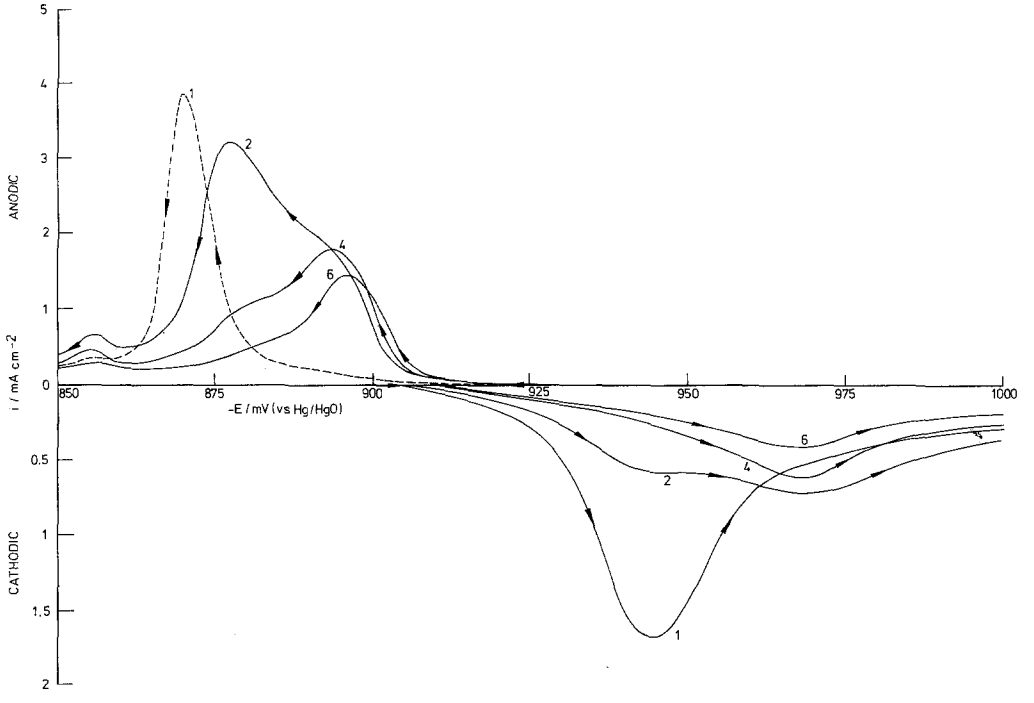

Fig. 7. Cyclic potential sweeps for planar cadmium electrode between −1000 and −850 mV; sweep speed 50 mV min^{-1}.

(The anodic and cathodic current scales are different in Figs. 6a, b, 7 and 8). This behaviour will be contrasted with the sintered electrodes in a subsequent section. Holding the potential at −750 mV after the anodic sweep for one hour prior to sweep reversal introduced a small cathodic prewave and delayed the main cathodic process (Fig. 6a). Breiter and Weinniger [12] attribute the prewave to the reduction of cadmium oxide on the thermodynamic reasonings of Lange and Ohse [26] that it cannot be the electroreduction of a hydroxide phase. Interestingly, the recent impedance studies [19] suggest that the anodic film at −700 mV, well into the passive region, has different characteristics to the initial passivating film at −870 mV. This may be a consequence of film thickening or a change in the nature of the film. Extension of anodic sweeps to −300 mV, Fig. 6b displayed similar cathodic features but maintaining the potential at the anodic extreme for 3 h enhanced the supposed formation of CdO. Under the conditions of the most extensive anodic excursion and stand period, Will [27] has demonstrated that γ-$Cd(OH)_2$, if formed, reverts to the more stable β-form. It therefore can be eliminated as contributing to the cathodic behaviour. No significant anodic process could be detected at −770 to −750 mV unlike in the case of the sintered electrode, presumably due to the absence of nickel.

Fig. 7 depicts the repetitive cycle behaviour in the region −1000 to −850 mV. The anodic peak initially divides but by six cycles reverts to a single peak displaced 25 mV cathodic to the original peak. After the first cathodic sweep, a considerable amount of unreduced hydroxide remains, and this explains the diminished anodic peak height on the subsequent anodic scan. The imbalance between charge and discharge is decreased with cycling. The new anodic peak could represent a second oxidation process, possibly the formation of γ-$Cd(OH)_2$; the potential at which it occurs eliminates CdO or CdO_2 as products. Will and Hess [2] have detected only small quantities of γ-$Cd(OH)_2$ during cycling which is inconsistent with the oxidation process involving this phase as it predominates in later cycles. The anodic peaks may represent the oxidation of bulk cadmium (less active) and finer cadmium deposited in the previous cathodic sweep from β-$Cd(OH)_2$. The cadmium crystallites formed on charge, especially at high

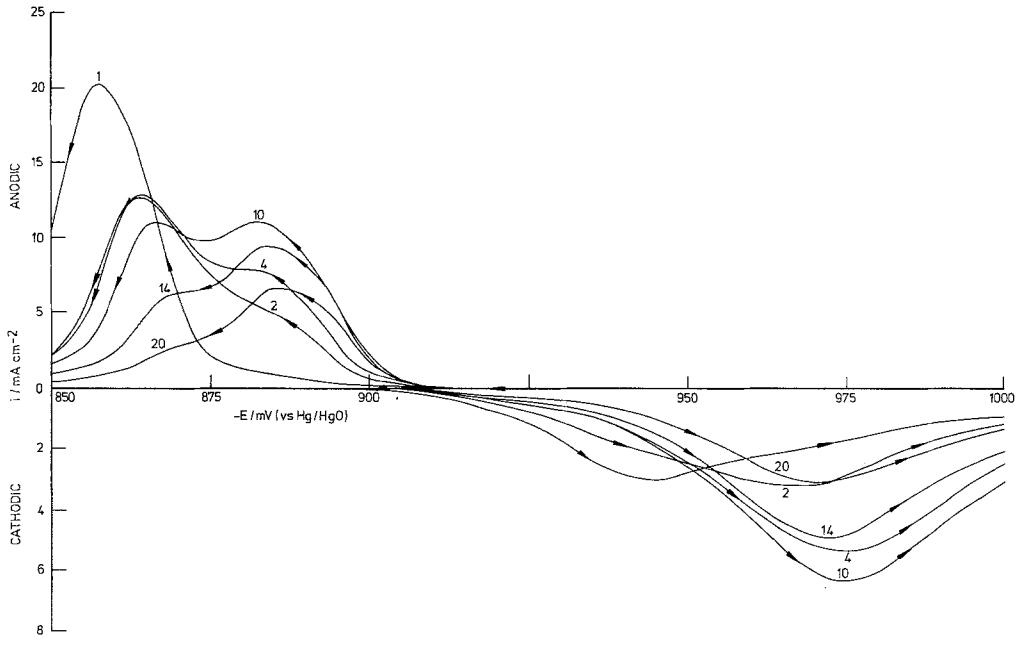

Fig. 8. Cyclic potential sweeps for planar cadmium electrode between −1000 and −850 mV; sweep speed 250 mV min^{-1}.

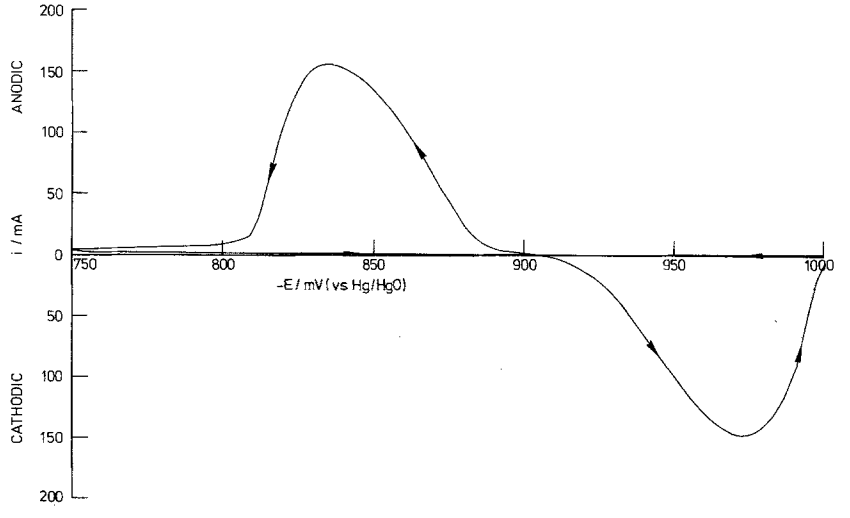

Fig. 9. First cycle potential sweep on charged ($C/2$ rate) sintered cadmium electrode; sweep speed 5 mV min^{-1}.

rates, are expected to undergo easier lattice dissolution as evidenced for zinc by Justinijanovic and Despic [29]. An alternative but less plausible explanation is that the double peak is caused by differing rates of nucleation of $Cd(OH)_2$ on the electrode surface. This fails to explain the absence of two peaks on the first anodic sweep. Maintenance of the potential at −1000 mV for 30 min between consecutive sweeps leads to a more complete reduction of the hydroxide and provides more bulk and finely divided cadmium and therefore larger anodic peaks. The electroreduction of $Cd(OH)_2$ is thought to proceed [11] via a low overpotential solid state mechanism and a higher overpotential solution species process. The first cathodic peak then relates primarily to the reduction of small β-$Cd(OH)_2$ crystallites in accordance with Will and Hess's observations, presumably by

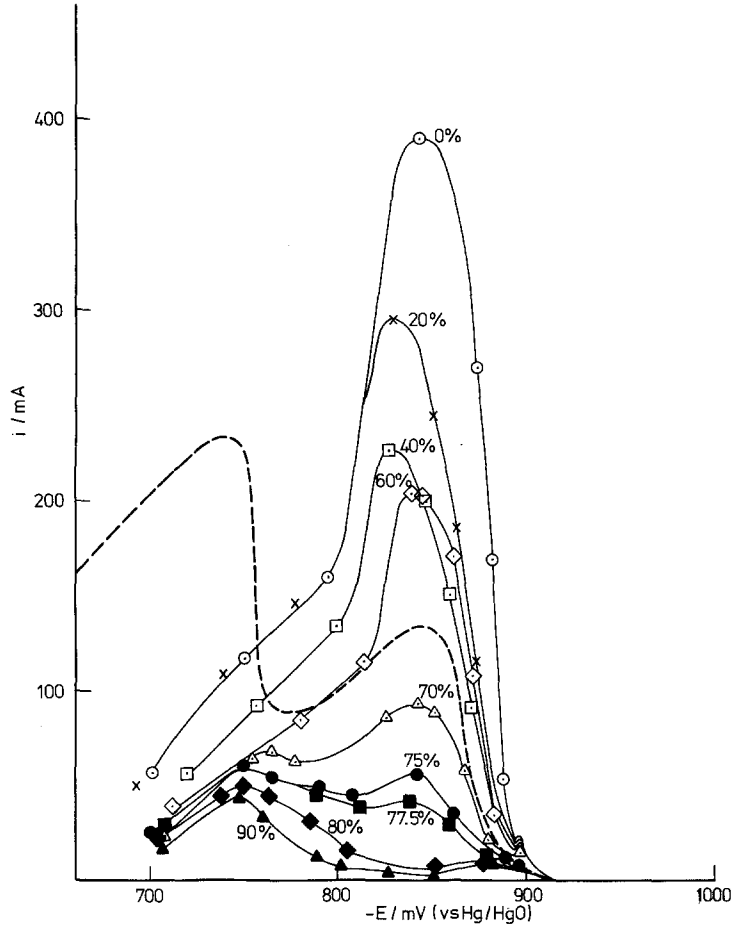

Fig. 10. Anodic potential sweeps on formed sintered cadmium electrode ($C/2$ charge for 16 h) after various extents of galvanostatic discharge at the $C/1$ rate; sweep speed 25 mV min^{-1}. ------ Anodic sweeps on an electrode containing initially 10% $Ni(OH)_2$ after 280 h overcharge ($C/2$ rate) at 75°C.

the solid state route. The cathodic displacement of the peak in subsequent cycles could reflect the involvement of the solution species or the build up in size of the hydroxide crystallites. Increasing the sweep speed five-fold resolved more clearly the anodic peaks (Fig. 8). The bulk cadmium oxidation peak decreased less rapidly with cycling whereas the more active increased in size up to ten cycles. The cathodic peaks exhibit a similar trend with cycling. This resulted from the more efficient reduction of the hydroxide at the faster sweep rate and the production of finer cadmium crystallites, in agreement with optical and analytical evidence presented previously for galvanostatic conditions of high charge rate [1].

3.3. *Potential sweeps on sintered electrodes*

Fig. 9 shows a slow scan cyclic sweep on a sintered electrode without ohmic corrections. The broadness of the peaks reflects potential distribution effects within the sinter. Comparison with planar electrode behaviour, Figs. 6–8, underline the increased charge acceptance of sintered plate cadmium electrode. This is due to the more intimate electrical contact between the nickel sinter current collector and active material and perhaps the lesser tendency to form larger $Cd(OH)_2$ crystals, at least in early cycle life. Fig. 10 shows the results of linear anodic sweeps on 'formed' electrodes containing 10% added $Ni(OH)_2$, previously subjected to increasing levels of galvanostatic discharge. The

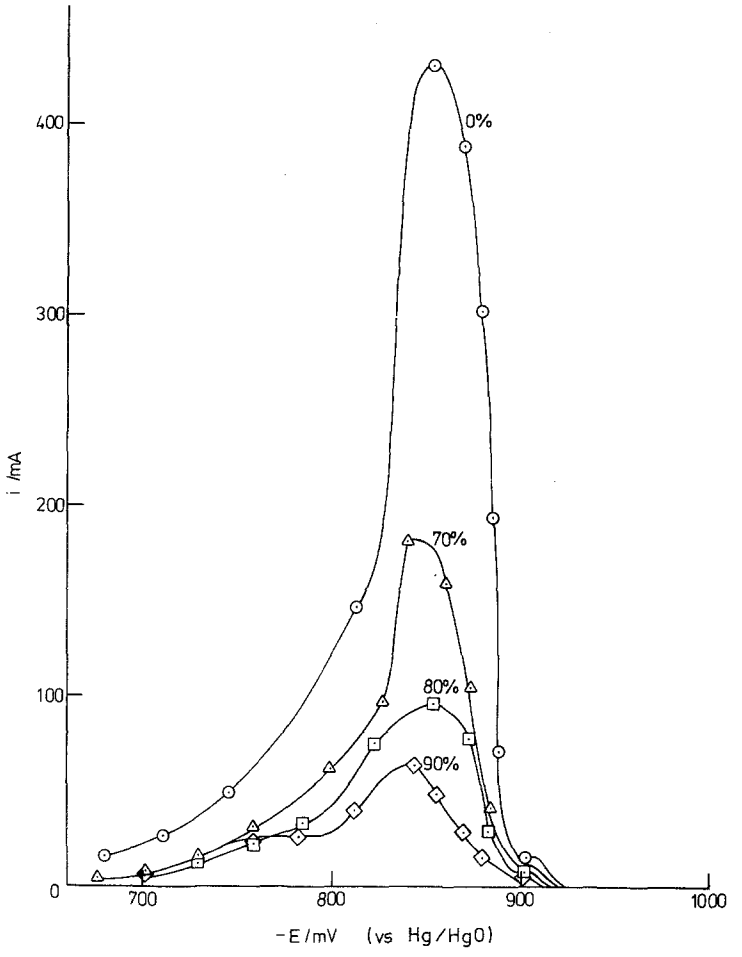

Fig. 11. Anodic potential sweeps on a cycled sintered cadmium electrode after various extents of galvanostatic discharge. Three cycles; $C/1$ charge rate; $C/1$ discharge rate; sweep speed 25 mV min^{-1}.

curves are corrected for iR drop. The usual peak at −840 to −860 mV is evident, corresponding with the consumption of active material and similar to that reported previously with one exception. The overall peak widths in this work are noticeably broader and it is suggested that the impregnation of the electrodes used previously was inferior. At greater depths of discharge an additional peak at −750 mV appears which is related to the discharge of the nickel-cadmium alloy. This is confirmed in Fig. 10 (broken line) which shows a sweep on an electrode containing initially 10% $Ni(OH)_2$ after being subjected to 280 hr overcharge ($C/2$ rate) at 75°C. The peak at −750 mV is now dominant and the relative peak heights at −750 and −860 mV correspond to the plateau lengths in Fig. 5. Electrodes containing low levels of $Ni(OH)_2$ impurity and subjected to little overcharge also gave small peaks at −750 mV. However, these were only seen when their associated charges were significant compared to the main anodic charge (after the bulk cadmium had been discharged). It should be noted that the peaks at −750 mV cannot arise simply from ohmic components related to the distribution of cadmium within the sinter, or to zoning of reaction rates of the Cd phase alone, because the peak position is independent of discharge current.

Fig. 11 shows a sequence of sweeps for an electrode (10% $Ni(OH)_2$) after three cycles at the $C/1$ charge and discharge rates. The electrode in the charged state was subjected to various levels of galvanostatic discharge as before. It is clear that the peak at −750 mV is much reduced, consistent with the observed shortening of the low potential plateau after galvanostatic cycling, (Fig. 3). The

initial peak height in Fig. 11 is very similar to that in Fig. 10 showing that at the high charge rate the reduction in cadmium surface area is small. In addition, the −860 mV peaks in Fig. 11 are narrower than in Fig. 10, which suggests a migration of cadmium metal towards the edges of the electrode (near to the Luggin capillary). This has been discussed recently [1] where it was concluded that redistribution and collection of active material within one part of the sinter matrix has a deleterious effect on electrode performance. The local pore volume per unit mass of active material diminishes and in extreme cases the electrode may resemble a planar one, cf. previous behaviour [4]. Thus at the high charge rate the fall in discharge capacity may be due largely to distribution rather than cadmium crystal growth effects. However, at low charge rates the growth of cadmium is also considerable.

4. Conclusions

(1) Discharge of planar and sintered cadmium electrodes follows a dissolution/precipitation process until a critical potential is reached at which passivation occurs.

(2) The hundred millivolt potential steps in the discharge curves of the sintered electrodes follow on the passivation of the major active material and reflect the probable presence of less active alloyed cadmium.

(3) The anodic behaviour of cycled planar electrodes involves the oxidation of bulk and electrodeposited cadmium, the latter being formed in previous cathodic scans.

(4) A further cathodic process is evident on planar electrodes after stand periods at potentials of −750 and −300 mV confirming the observations of Okinaka [11] and Breiter and Weinniger [12]. The reduction may correspond with the removal of the original passivating film which has thickened and is more easily detectable or a chemically different anodic product/film.

(5) The better charge acceptance of sintered electrodes compared with planar ones is clearly demonstrated.

Acknowledgements

The authors appreciate the helpful discussions with Dr R. D. Armstrong. This work forms part of a collaborative project with Newcastle University. The experimental contributions of Mr R. M. Coughlan and Mr G. T. Crickmore are acknowledged together with the Directors of Ever Ready Co. (Holdings) Ltd. for permission to publish.

References

[1] R. Barnard, J. A. Lee, A. H. Rafinski and F. L. Tye, 'Power Sources 5' (Ed. D. H. Collins), Academic Press, London (1975) pp. 183–209.
[2] F. G. Will and H. J. Hess, *J. Electrochem. Soc.* **120** (1973) 1.
[3] J. P. Harivel, B. Morignat and J. Migeon, 'Batteries' Vol. 2 (Ed. D. H. Collins), Pergamon Press, Oxford (1965) p. 107.
[4] R. D. Armstrong, A. D. Sperrin, F. L. Tye and G. D. West, *J. Appl. Electrochem.* **2** (1972) 265.
[5] E. J. Casey and J. B. Vergette, *Electrochim. Acta,* **14** (1969) 897.
[6] F. Przybyla, G. R. Ramsey and T. C. O'Nan, 'Power Sources 4' (Ed. D. H. Collins), Oriel Press, Newcastle (1973) pp. 401–414.
[7] J. S. Dunning, D. N. Bennion and J. Newman, *J. Electrochem. Soc.* **120** (1973) 906.
[8] P. Bro and H. Y. Kang, *ibid.*, **117** (1971) 583.
[9] P. Selanger, *J. Appl. Electrochem.* **4** (1974) 249.
[10] R. D. Armstrong and G. D. West, *J. Electroanal. Chem.* **30** (1971) 385.
[11] Y. Okinaka, *J. Electrochem. Soc.* **117** (1970) 289.
[12] M. W. Breiter and J. L. Weinniger. *ibid.*, **113** (1969) 651.
[13] M. A. V. Devanathan and S. Lakshmanan, *Electrochim. Acta* **13** (1968) 667.
[14] A. Fleischer, *J. Electrochem. Soc.* **94** (1948) 289.
[15] L. Horn, *Chem.-Ing.-Techn.* **38** (1966) 660.
[16] P. Delahay, 'New Instrumental Methods in Electrochemistry', Interscience, New York (1954) p. 133.
[17] K. Appelt, 'Batteries' Vol. 2, (Ed. D. H. Collins), Pergamon Press (1965) pp. 93–105.
[18] G. D. West, Ph.D. Thesis, Newcastle University (1972).
[19] R. D. Armstrong and K. Edmondson, *J. Electroanal. Chem.* **53** (1974) 371.
[20] S. U. Falk, *J. Electrochem Soc.* **107** (1960) 661.
[21] R. Barnard, unpublished work.
[22] Yu. M. Pozin, and N. K. Terent'ev, *Zh. Prikl. Khim.* **46** (L) (1973).
[23] V. I. Levina, and S. A. Rozentsveig, *Advances in Storage Battery Manufacture Vses, Nauchn.-Issled, Inst. Elektromekhan., Moscow* **2** (1964) 10.
[24] W. Ekman, *Z. Phys. Chem.* **12** (1931) 69.
[25] D. M. Kolb, M. Przasnyski and H. Gerischer, *J. Electroanal. Chem.* **54** (1974) 25.
[26] E. Lange and R. Ohse, *Naturwiss.* **45** (1958) 437.
[27] F. G. Will, *Extended Abstracts, Batt. Electrochem. Soc.*, Fall Meeting, Detroit (1969) p. 62.
[28] I. N. Justinijanovic and A. R. Despic, *Electrochimica Acta.* **18** (1973) 709.
[29] J. S. Dunning, D. N. Bennion and J. Newman, *J. Electrochem. Soc.* **118** (1971) 1251.